



OPEN

Earthquake-induced soil landslides: volume estimates and uncertainties with the existing scaling exponents

Ali P. Yunus^{1,8}, Chen Xinyu^{2,8}, Filippo Catani³, Srikrishnan Siva Subramaniam⁴, Xuanmei Fan⁵, Dou Jie⁶, K. S. Sajinkumar⁷, Ankita Gupta² & Ram Avtar²✉

Quantifying landslide volumes in earthquake affected areas is critical to understand the orogenic processes and their surface effects at different spatio-temporal scales. Here, we build an accurate scaling relationship to estimate the volume of shallow soil landslides based on 1 m pre- and post-event LiDAR elevation models. On compiling an inventory of 1719 landslides for 2018 M_w 6.6 Hokkaido-Iburi earthquake epicentral region, we find that the volume of soil landslides can be estimated by $\gamma = 1.15$. The total volume of eroded debris from Hokkaido-Iburi catchments based on this new scaling relationship is estimated as 64–72 million m³. Based on the GNSS data approximation, we noticed that the co-seismic uplift volume is smaller than the eroded volume, suggesting that frequent large earthquakes (and rainfall extremes) may be counterbalancing the topographic uplift through erosion by landslides, especially in humid landscapes such as Japan, where soil properties are rather weak.

Strong seismic shaking in a steep mountain belt induces hundreds to thousands of landslides, thereby eroding the topography instantaneously¹. Quantifying the volume of earthquake-induced landslides (EQIL) is critical to understand the topographic evolution and mountain building processes², mass wasting and sediment budget^{3,4}, reservoir siltation⁵, to ascertain chains of geohazard risk in downstream patches including debris flows and floods^{6,7}, vegetation dynamics and carbon sink^{8–10}, and other atmospheric and surface processes¹¹. However, only a limited number of studies succeeded in accurately quantifying EQIL volumes immediately following a seismic event¹². A number of reasons may explain the paucity of landslide volume studies: (1) the three-dimensional nature of the object landslide that is, conversely, intrinsically mapped as two-dimensional, (2) inaccessible terrains, (3) impractical to quantify huge debris piles in field measurements, (4) lack of high-resolution pre-event topographic information, and (5) total and partial reactivations of landslides that may merge sediment volumes pertaining to different triggering events^{13,14}.

There exist several practical examples of estimating landslide volumes that rely on empirical power-law relationships between the area of a landslide and its volume^{2,15,16}. Although area (*A*) can be easily obtained from a landslide inventory map, volume (*V*) typically requires a small amount of field component or accurate pre- and post-event topographic data to finally compute the scaling exponent γ and intercept α in the equation $V = \alpha A^\gamma$ ¹⁷. Literature suggests that the major source of uncertainty in the volume estimation comes from the uncertainty in the parameter γ ^{2,18}. The value of γ is reported to be in the range of $1.0 \leq \gamma \leq 1.9$ for a volume sizes of 10^2 m³ to 10^3 m³¹⁹.

Empirical models for volume estimation originated four decades ago¹⁷, but the large uncertainties arising from the material differences and the lack of validation data caused researchers to be cautious while employing the results for practical use. Significant errors in the early scaling relationship may be accounted for by the underdeveloped remote sensing and GIS technologies at that time²⁰. Before the availability of multi-temporal high-resolution digital elevation models (DEM), reliable scaling relationships were therefore dependent on the possibility to execute intensive and expensive field surveys. Despite the difficulty, Imaizumi et al.²¹ measured

¹Department of Earth and Environmental Sciences, Indian Institute of Science Education and Research Mohali, Mohali, Punjab 140-306, India. ²Faculty of Environmental Earth Science, Hokkaido University, Sapporo 060-0810, Japan. ³Department of Geosciences, University of Padova, 35131 Padova, Italy. ⁴Centre of Excellence in Disaster Mitigation and Management, Indian Institute of Technology Roorkee, Roorkee, Uttarakhand 247667, India. ⁵State Key Laboratory of Geohazard Prevention and Geoenvironment Protection, Chengdu University of Technology, Chengdu, People's Republic of China. ⁶Three Gorges Research Center for Geohazards, The China University of Geosciences, Wuhan 430074, People's Republic of China. ⁷Department of Geology, University of Kerala, Thiruvananthapuram, Kerala 695 581, India. ⁸These authors contributed equally: Ali P. Yunus and Chen Xinyu. ✉email: ram@ees.hokudai.ac.jp

51 rainfall-induced landslide scars in the field with sizes ranging from 10 m² to 3000 m², and came up with a scaling exponent of $\gamma = 1.31$. But in the case of EQIL, the number and size of landslides are much larger, and hence the difficulties in executing an accurate field measurement are often overwhelming. Regardless of their high accuracy, conventional measurements in field surveys are limited to landslide sizes of some extent, mainly owing to inaccessibility to climb-up to the scar regions in mountain terrains.

With the advancement in GIS and Earth Observation technologies, more scaling relationships based on remote measurements have been proposed. Massey et al.¹² analyzed a catalogue of 17,256 landslides triggered by the M_w 7.8 Kaikōura, earthquake, New Zealand using DEMs generated from stereo aerial photographs, and found a scaling exponent $\gamma = 1.109$ for all the landslides and 1.13 ± 0.03 for soil landslides alone. Nevertheless, the classification of the debris into different material types and units yielded different scaling exponents, suggesting that different scaling exponents are needed for soil, bedrock, and mixed (soil–bedrock) landslides.

Researchers have noticed regional differences in scaling relationships for soil landslides, depending on the thickness of the regolith²². Larsen et al., (2010) reported that the lowest γ -values are found for soil landslide in glaciated and semi-arid regions, where soil formation is thin compared to the thick soil layers to be found in temperate and tropical regions. In loess deposits, for instance the landslides in Chinese Loess Plateau, the γ -values are found similar to soil landslides found in tropical and temperate region because of thick layering²³. For such reasons, it is imperative to develop accurate landslide volume estimates for each earthquake inventory. Moreover, the peculiar topography of Iburi in Hokkaido prefecture, comprising multiple tephra layers some several meters deep, is worthy of attention.

In this paper, we develop a volume-area relationship for landslides triggered by the 2018 M_w 6.6 Hokkaido Eastern Iburi Earthquake derived from high-resolution LiDAR DEMs. Using the scaling relationship, we quantify the total volume of eroded materials from the hillslopes of the entire affected areas. As far as the authors know, the selected study site is probably the only case where EQIL debris are completely or near completely moved out of hillslopes because of their low relief and gentle topography; hence, the area-volume relationship presented in this work can be useful globally for accurate soil-landslide volume estimates. In addition, we investigate the uncertainties in existing scaling relationships and their influence on total volume estimates. From these results, we briefly discuss how large earthquakes may counterbalance the topographic uplift in terms of net rates of sediment volume change.

In tectonically active areas, thrust faulting earthquakes progressively increases the steepness and height of mountain ranges^{24,25}. For example, M_w 7.8 Gorkha earthquake generated about 1 m of uplift in the Kathmandu Basin, which is overall one order of magnitude higher than the erosional processes by landslides²⁶. However, a few studies have demonstrated the impact of large earthquakes on high magnitude topographic erosion through landslides, raising fundamental questions concerning orogenic processes. For instance, analysis of EQIL data from M_w 7.9 Wenchuan shows that this earthquake event dominates the erosional budget³. We therefore aim to estimate the net volume balance associated to the 2018 Hokkaido-Iburi earthquake from landslide volume analysis. This is important because it also reveals how different magnitude earthquakes behave in different topographies in terms of erosion and uplift, and can contribute to the overall understanding on the mountain building processes.

Materials and methods

The September 6, 2018 Hokkaido Eastern Iburi M_w 6.6 (M_j 6.7) earthquake triggered about 10,120 landslides²⁷, mostly shallow soil slides, spanning a geographical area of ~ 500 km² (Fig. 1). Following the earthquake, several landslide inventories were created for this event with the landslides number ranging from three thousand to more than ten thousand failure surfaces^{27–31}. The large variation in the number of landslides mapped in different inventories is due to the difference in the mapping criteria adopted. For example, the Geospatial Information Authority of Japan (GSI), manually mapped the landslides from 0.5 m aerial photos and their inventory contains 3307 landslide polygons; this number is much fewer than other inventories, because GSI combined several small landslides in the same slope aspect into a large single landslide. Wang et al. (2018) digitized 7941 landslide polygons by comparing pre- and post-event 3.7 m resolution Planet images, and Dou et al. (2020), manually delineated 10,120 landslide polygons based on 0.5 m aerial photos and 2 m DEM for avoiding the shadow effect, and further to separate many clustered landslides into several smaller ones (see Supplementary Fig. S1). Accordingly, the total landslide area varies from 26.07 km²²⁸ to 27.97²⁷ to 48.77²⁸ km².

Completeness of mapping assessment for these three inventories was verified by searching for landslides in the neighboring zones using large swath images collected by Landsat 8 OLI and Sentinel-2 satellite after the earthquake. On the other hand, mapping accuracies varies from interpreter to interpreter; but avoidance of non-coseismic landslides is achieved by performing manual cross-checking with pre-earthquake images. Since there is a large difference in both the number and area of landslides, we used all the three aforementioned open inventories to approximate the total volume of materials eroded from the study area catchments and to quantify the uncertainties in landslide mapping.

Surface geology in the study area is comprised of volcanic pumice fall deposits from Tarumae (~ 9000 years ago), Eniwa ($\sim 20,000$ years ago), and Shikotsu ($\sim 46,000$ years ago) volcano, having a soil thickness of 0.85 m to 2.65 m^{32,33}. Osanai et al. (2019) reported that the topsoil layer in the middle of the failed slope reaches a thickness of 2.5–3.5 m. In places, the volcanic soil deposits are even deeper than 8 m³⁴. Additionally, the data from global 1-km gridded thickness of soil, regolith, and sedimentary deposit layers³⁵ show an average thickness of 2.93 m in the calibration region.

High resolution (1 m) LiDAR DEMs for pre-earthquake and post-earthquake periods were obtained from the Hokkaido Provincial Government. The pre-earthquake LiDAR DEM was developed for the purpose of Atsuma Dam Construction in 2012 by the Construction Management Department of the Atsuma district in the

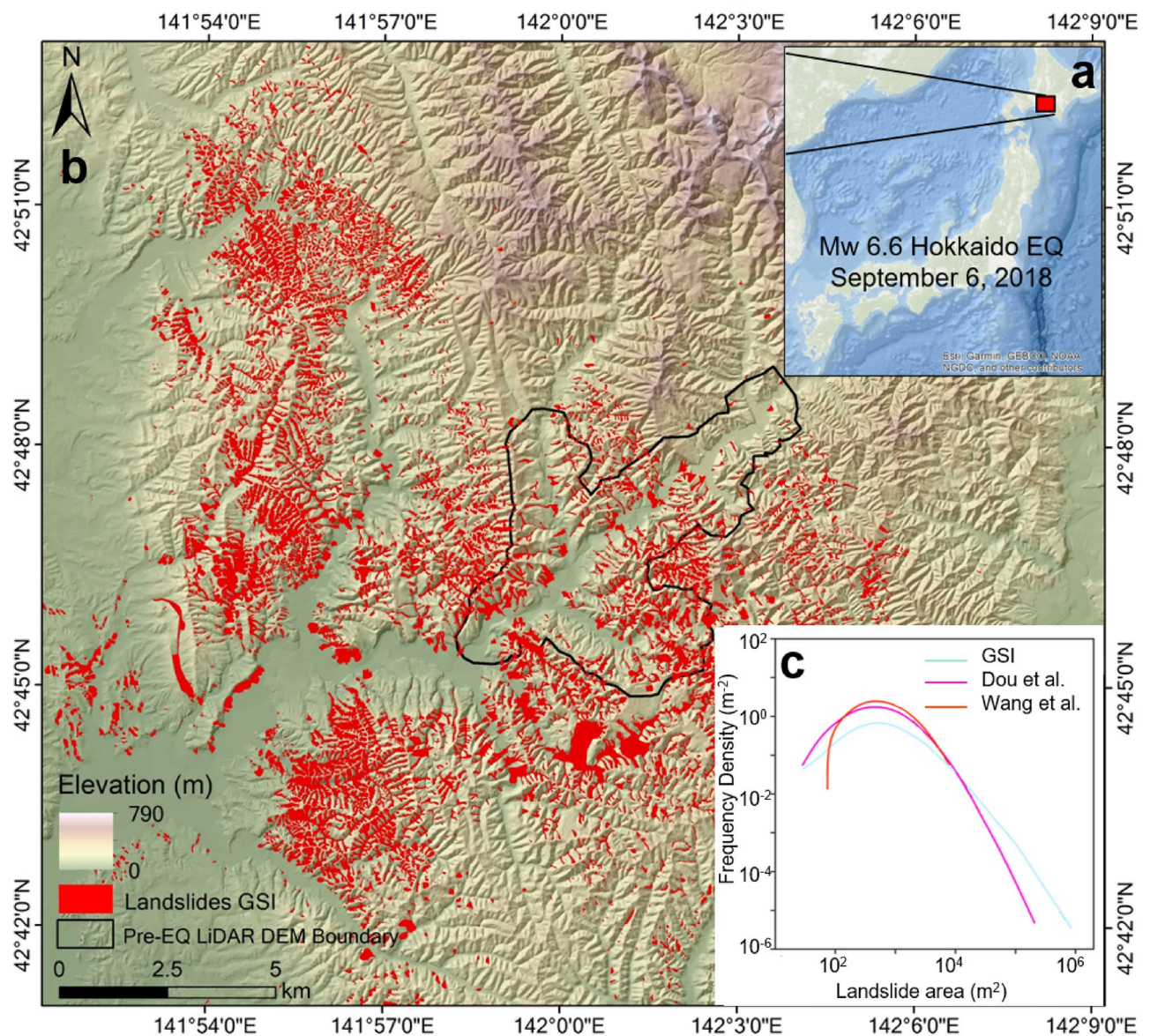


Figure 1. (a) Location map of Hokkaido Eastern Iburu M_w 6.6 earthquake epicentral area, (b) showing the location of landslides mapped by GSI (red shaded areas);. Calibration area, i.e., the areal extent of 1 m pre and post event DEM availability are shown in black polygon. (c) shows the frequency density-landslide area plot for three different inventories (GSI—blue line, Dou et al. 2020—pink line, and Wang et al. 2019—orange line).

EPSG2454 JGD2000 coordinate system. Following the earthquake in 2018, the Forestry Division of the Atsuma district carried out a survey for obtaining the post-event LiDAR DEM in the same coordinate system. While the total area covered in the pre-earthquake survey was only 29.41 km² (hereafter refer as calibration area), the post-earthquake survey was about 512 km² (hereafter refer as testing area), i.e., ~95% of the total earthquake-affected area. The accuracy of both DEMs has been evaluated on the basis of a total of 350 random points selected from the non-landslide areas (supplementary Fig. S2) resulting in a root mean square error of 0.37 m, a mean absolute error of 0.31 m in elevation, and $R^2 = 1$ when considering 2012 DEM as reference data. Such accuracy is better than that were used in previous similar studies and is therefore suitable for our purpose. For instance Tang et al.¹⁵ by analysing landslide volumes using multi-source DEMs concluded that high resolution DEMs provides more realistic estimates than the low resolution ones, and those with larger bias.

While the three available landslide inventories are used for quantifying the total landslide volume, we additionally created a new database of landslides in the calibration area (i.e., the 29.41 km² coverage area of pre-earthquake LiDAR data) for developing a specific area-volume relationship. This database is created by the DEM subtraction method and identifies areas with negative changes in the elevation. By automated GIS techniques (Fig. S3, supplementary file), these negative-change areas are then mapped as landslide source zones and extracted for the area and volume analysis (Fig. 2). The automatically extracted landslides are manually cross verified with the aerial photographs (0.5 m; taken in 2018) for any inaccuracy, and if found they are manually edited

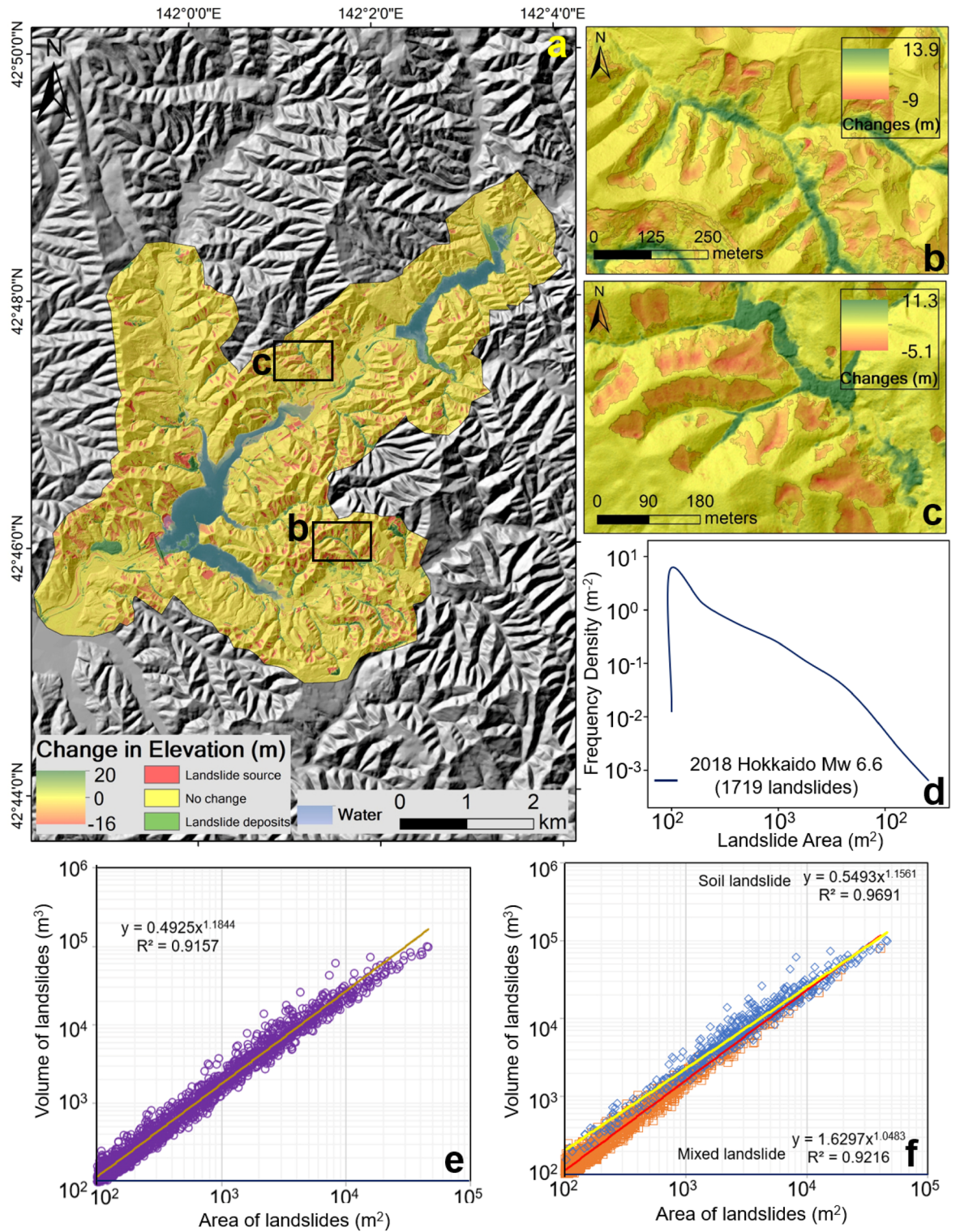


Figure 2. (a) Post and pre-event LiDAR DEM subtraction map showing changes in elevation values caused by landslides; red shows areas of landslide source and green shows deposition zones. (b) and (c) are the enlarged areas of rectangles shown in (a). (d) Shows the frequency density—landslide area plot for the 1719 landslides mapped by DEM subtraction. Correlations between landslide area and landslide volume for (e) all 1719 landslides and (f) shows the distinction in correlation values between soil landslides and mixed soil-bedrock landslides.

in a GIS. As many as 50 landslides were visited in the field to observe the hillslope debris and to validate DEM subtraction figures.

A laser range finder (Nikon coolshot 40i), was pointed to the side walls and crown portions of landslide body to approximate the depth values. Because of the relatively small relief (average = 31 m and maximum = 201 m), almost all the landslide debris has been removed to the valley bottom. The main geometrical features (length and width) of newly mapped landslides from DEM subtraction method were extracted by specifying minimum convex hull bounding geometry enclosing the landslide polygon. Length and width are then estimated from the longest and shortest distance between any two vertices of the convex hull (Taylor et al., 2018). The area of landslides is calculated by means of the *Calculate Geometry* tool that populates the geometric values derived from landslide polygon features based on data frame's coordinate system in ArcGIS. The volumes and depths of these landslide source areas are computed by spatially aggregating sums of DEM-subtraction pixels within the landslide polygons using the following equation:

$$V = A \sum_{x=1}^n S \quad (1)$$

where V is the volume, A is the cell area in 3D, S is the subtracted value from pre-event DEM and post-event DEM for each cell, and n is the cell count.

Further, to examine the landslide area-volume relationship, a relative volume-area scaling for the landslides in the study area was assessed based on the following equation²²:

$$V = \alpha A^\gamma \quad (2)$$

where V is the landslide volume, A is the landslide area, α is the intercept, and γ is the scaling exponent. To investigate and discuss the uncertainties in existing scaling relationships and their influence on total volume estimates, we then compare the results of our area-volume relationships obtained using the newly mapped 1719 landslides from the calibration area, with existing scaling coefficients available in the literature (Table 1).

Lastly, to compare co-seismic landslide-induced volume losses with tectonically driven volume gains in the landscape, we establish uplift rates produced by the M_w 6.6 Hokkaido Eastern Iwate Earthquake for the study area using the following method. GSI estimated the ground displacement caused by the earthquake and modelled the fault slip position by employing ALOS-2 SAR (DAICHI-2) data acquired before and after the earthquake together with data from the global satellite navigation system (GNSS) (GSI, 2018). We georeferenced the published vertical component map and interpolated the uplift values obtained from 11 GNSS stations (co-seismic uplift rate ranging from 0 to 3.65 cm) using the inverse distance weighted (IDW) technique (Supplementary Fig. S4), and calculated the net uplift volume caused by this M_w 6.6 earthquake. It is worth mentioning that our calculation of net uplift volume only covers the size of post-earthquake DEM (Fig. S3). The volume of uplift is calculated by using Parker et al. formula:

$$V_u = A \sum_{x=1}^n U_x \quad (3)$$

where V_u is the net uplift volume, A is the cell area, U_x , the vertical displacement for each cell, and n is the cell count.

Dataset	Log10 α	γ	R ²	n	References
Global	-0.836 ± 0.015	1.332 ± 0.005	0.95	4,231	²²
Global	-1.131	1.45 ± 0.009	0.97	677	³⁶
Global bedrock	-0.73 ± 0.06	1.35 ± 0.01	0.96	604	²²
Global soil	-0.44 ± 0.02	1.145 ± 0.008	0.90	2136	²²
Japan soil	-0.41	1.31	0.84	51	²¹
Japan soil	-0.72	1.19	0.86	11	³⁷
Japan mixed	-0.60 ± 0.06	1.36 ± 0.03	0.88	236	²²
Himalayas soil	-0.44 ± 0.07	1.25 ± 0.03	0.92	141	²²
Himalayas mixed	-0.59 ± 0.03	1.36 ± 0.01	0.98	428	²²
Himalayas bedrock	-0.49 ± 0.08	1.34 ± 0.02	0.98	123	²²
New Zealand (all)	-0.86 ± 0.05	1.36 ± 0.01	0.97	389	²²
New Zealand (all)	-0.05	1.109	0.68	8442	¹²
New Zealand soil	-0.37 ± 0.06	1.13 ± 0.03	0.86	237	²²
New Zealand soil	0.12	1.060	0.69	1824	¹²
New Zealand Mixed	-0.86 ± 0.05	1.36 ± 0.01	0.97	389	²²
New Zealand bedrock	-0.13	1.138	0.67	6618	¹²
China, Wenchuan	-0.975	1.388	-	41	³
China, Wenchuan	0.119	1.209	0.78	1415	²⁰
Korea	-0.229	1.02	0.89	930	³⁸

Table 1. Landslide area and volume scaling relationships available in the literature.

Results

A total of 1719 landslides are mapped in the calibration area. Area and volume of landslides vary widely in the calibration area. To minimise uncertainties in the landslide area mapping and volume estimation, we considered the smallest landslide area as 100 m^2 in the analysis. The frequency density plot, as expected, exhibits characteristic power-law scaling (Fig. 2f). The largest mapped landslide in calibration area is $45,978 \text{ m}^2$, the mean is 1995 m^2 and the standard deviation is 4166 m^2 . The smallest landslide volume mapped in calibration area is 84 m^3 and the largest is $10 \times 10^4 \text{ m}^3$. The mean mapped volume is 4611 m^3 , with a standard deviation of $10,138 \text{ m}^3$. The range of landslide depth varies from 0.45 to 24.42 m , with a mean depth of 1.72 m . The total landslide area and volume in the calibration zone are $3.43 \times 10^6 \text{ m}^2$ and $7.92 \times 10^6 \text{ m}^3$, respectively. It is noteworthy to mention that the areas with positive changes (3.30 km^2 , i.e., the landslide deposits) nearly equals the areas with negative changes (3.43 km^2). We presume that a small part of debris materials might have been washed out of the catchment.

Geometrical properties such as landslide area (A), the maximum length of landslide (L), the maximum width of landslide (W), and maximum depth (H) for the 1719 landslides are correlated with the mapped volume obtained from DEM subtraction and focal statistics method. Log-transformed regression curves for the correlation plot are presented in (Fig. 2, and Supplementary S5). The R^2 , i.e., coefficients of determination for the landslide area and volume, length and volume, width and volume, and depth and volume are 0.91 , 0.78 , 0.78 , and 0.19 , respectively. As expected, the best fit correlation is obtained for landslide area and volume (Fig. 2).

Landslide area-volume relationship. The landslide area-volume scaling relationship for the 1719 landslides in the study site is defined as $V = 0.49 \times A^{1.18}$ ($R^2 = 0.91$; $N = 1719$) (Fig. 2). Based on our field surveys, and published literature^{39,40}, most EQILs are classified as shallow soil landslides (supplementary Fig. S6). Only a few landslides have failure surfaces that have exposed bedrocks and soil layers that extend deep (Fig. 3)^{32–34}. The slip surface of these shallow landslides is either the weathered tephra layer or the basement sedimentary complex. Since the failure surface in the study area is about 2.5 – 3.5 m in most cases, we extracted the landslides having a depth less than 3.5 m ($n = 1187$), and considered them as purely soil landslides. The remaining landslides ($n = 532$), with a depth ranging between 3.50 and 24.12 m , are classified as mixed soil–bedrock landslides. The scaling relationship for soil and mixed landslide from area-volume analysis therefore are $V = 0.54 \times A^{1.15}$ ($R^2 = 0.97$) and $V = 1.62 \times A^{1.04}$ ($R^2 = 0.92$), respectively (Fig. 2).

Volume of debris generated during the Hokkaido earthquake. Based on the area-volume scaling relationship obtained from the calibration area, we estimate the total volume of earthquake-induced landslide for the Hokkaido Eastern Iburi earthquake for the three different inventories. The estimated total volume of debris for the Hokkaido Eastern Iburi earthquake, derived based on the Wang et al.²⁸ inventory, is 56.17 million

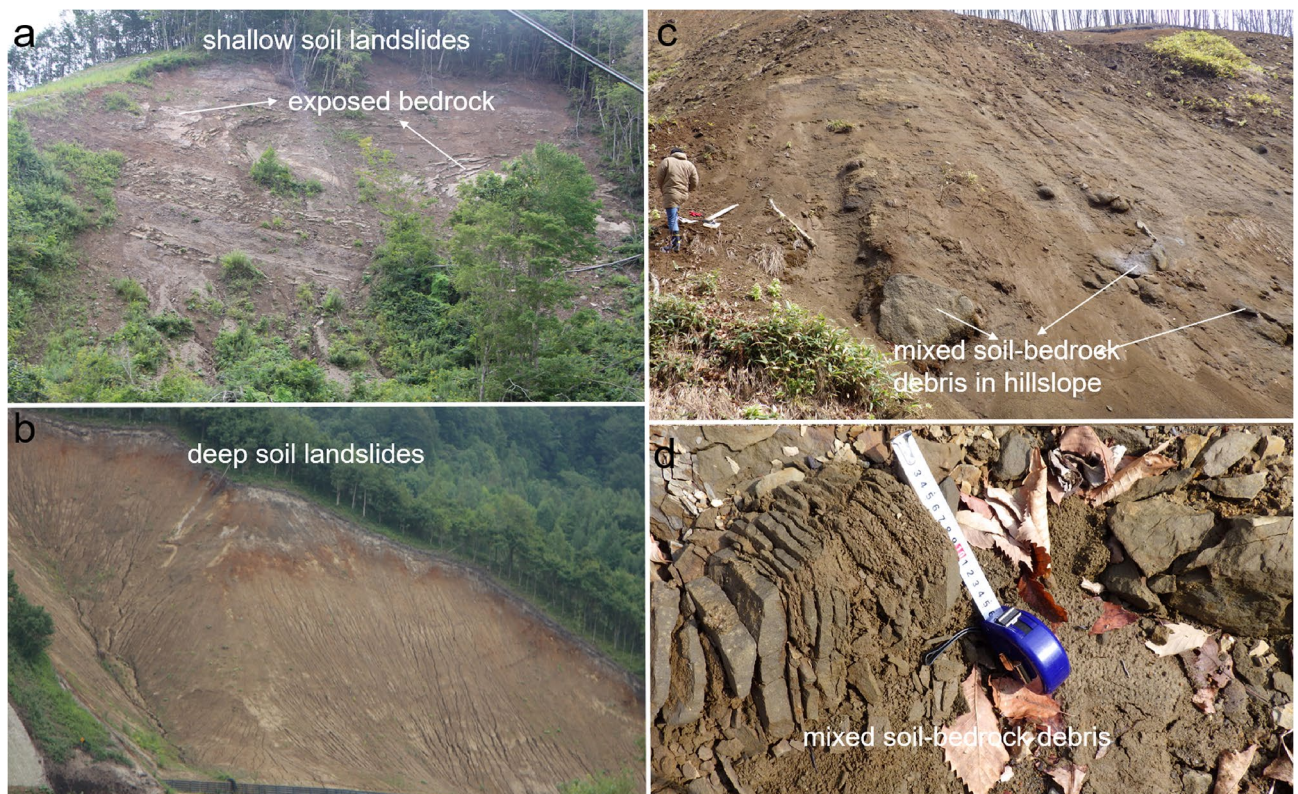


Figure 3. (a) Shallow soil landslides exposing bedrock in steep slopes, (b) deep soil landslides, (c) debris with fragments of boulders in lower hillslopes, and (d) mixed soil bedrock debris in the valley.

m³ for soil landslides and 64.75 million m³ for all landslides, whereas Dou et al.²⁷ inventory give a volume of 64.72 million m³ and 75.61 million m³, respectively. The largest volume was obtained with the GSI (2018) inventory, i.e., 157.87 million m³ and 197.72 million m³.

Discussion

Based on the landslide area-volume relationships, we estimate that approximately 56–197 million m³ of debris materials were removed from the low-relief Hokkaido-Iburi region after the earthquake. Estimates of the volume of landslides associated with the Wang et al.²⁸ mapping are about 8.55–10.86 million m³ lower than Dou et al.²⁷, while those mapped by GSI are about two times higher (~93–122 million m³) than Dou et al.²⁷, a difference that may be attributed at least in part to mapping uncertainty. The large differences in estimated volumes demonstrate that landslide areas not divided into their source and deposition areas can strongly produce bias in volume estimates, as the relationship linking area to volume is not linear. Additionally, the degree of accuracy in the separation of multiple overlapping landslide boundaries on the same slopes, i.e., the ability to differentiate individual landslides from clustered landslides may also lead to a significant improvement in the volume estimate (Fig. S1). For example, Massey et al. (2020) reported that the amalgamation of small landslides into a single one can inflate volume by up to a factor of three.

We notice that the volume of landslides calculated from the DEM subtraction method (i.e., 7.92×10^6 m³) in the calibration area has a close match with the Dou et al. (2020) landslide inventory (7.47×10^6 m³) than with the other two inventories (GSI = 14.88×10^6 m³ and Wang = 6.54×10^6 m³). The highest accuracy found in Dou et al.²⁷ inventory may be attributed to their mapping pattern as their database is the only one that separates source areas from deposition areas, reducing the amalgamation bias. Therefore, this inventory has been used in the uncertainty analysis of existing scaling relationships.

Uncertainties in the existing scaling relationships. The preliminary estimate of the Ministry of Land, Infrastructure, Transport, and Tourism of Japan indicates that the total volume of debris generated by the 2018 Hokkaido Eastern Iburi Earthquake is about 30 million m³⁴¹. Our results suggest that the total debris volume triggered by the M_w 6.6 quake is anywhere between 64 and 75 million m³ (Fig. 4b); suggesting that the initial estimates underrated the total sediment volume from the affected catchments⁴¹. However, such large uncertainties may have consequences in a post-hazard scenario setting. For instance, we noticed that a few check dams constructed in the region to arrest the sediment flow were full within 3 years after the event (see supplementary Fig. S7). As an example, during the Wenchuan earthquake, the landslides produced approximately 2.6×10^9 m³ of debris deposited on the hillslopes and valleys in the entire affected area (~13,800 km²)^{3,42}, providing abundant sources for debris flows.

A decade after the Wenchuan earthquake, catastrophic debris flows remain a looming threat in the Wenchuan catchments⁴³. Therefore, reliable estimates of sediment volume still available on slopes are a necessary first step required for the development of post-hazard mitigation strategies based on post-seismic residual risk, as well as for calibrating sediment budget models. Since area mapping of landslides can be easily and quickly done with the help of optical remote sensing techniques^{43,44}, a quick workaround for volume estimation based on an accurate scaling coefficient is the optimal approach for most uses. To better ascertain the degree of accuracy of our empirical relation, we compared the existing models on volume determination with our results based on Dou et al. (2020) inventory (Fig. 4).

The coefficient α obtained for soil landslides in this study is 0.49–0.55, whereas the exponent γ is 1.15–1.18. The γ values of 1.15–1.18 indicate that the depth of the landslides in the region is almost uniform, which is confirmed by our field observations. In other soil landslide area-volume relationships^{21,22,37}, a smaller α coefficient is noticed (0.19–0.48), whereas γ values widely range from 1.11 to 1.31, with an average of 1.18, indicating that γ values obtained in this study for landslides initiated by the Hokkaido Eastern Iburi earthquake are well within the range reported in the literature (Fig. 4a). On the other hand, the α coefficient obtained for soil landslides mapped for New Zealand that used a high-resolution dataset for volume mapping was found to be on the higher end ($\alpha = 1.31$) with a lower γ value ($\gamma = 1.06$)¹². However, despite the large difference in α and γ , the total volume of landslides mapped for Hokkaido earthquake estimated from this study and the area-volume relationship of Massey et al.¹² are found similar to each other (Fig. 4b).

The significant difference in a large number of small landslides mapped in the Kaikoura inventory perhaps caused the differences in the coefficients (see Supplementary Fig. S8). All other soil landslide scaling relationships except two underestimated the volume values. The scaling relationships derived from Imaizumi and Sidle (2007) and Imaizumi et al. (2008) overestimated the volume, possibly because of the limited number of samples ($n = 51$ and $n = 11$) used in the analysis. Additionally, the landslides reported in these two studies are precipitation induced. The good match in volume values obtained for Hokkaido earthquake induced landslides from our relationship and that from Massey et al.¹² relationship could be related to the high accuracies of the mapping measurement used. Moreover, like the Hokkaido Eastern Iburi co-seismic landslides, the Kaikoura inventory also contains a high proportion of shallow soil failures¹.

Co-seismic net uplift and erosion volume. Apart from the mountain-building process in the form of continuous uplift, another fundamental concept of orogenic evolution is that mountains are built through recurring cycles of vertical uplifts by earthquakes⁴⁵. This process was questioned in Parker et al.³, that discuss whether large earthquakes create or destroy mountainous topography. By analysing the landslides triggered by the 2008 M_w 7.9 Wenchuan earthquake, their study shows that co-seismic landslide volume (~5–15 km³) is about 2 to 6 times greater than co-seismic uplift volume (~2.6 km³), thus suggesting the need for careful consideration of the role of co-seismic uplift-erosion balance in topographic development. Nevertheless, the Wenchuan earthquake

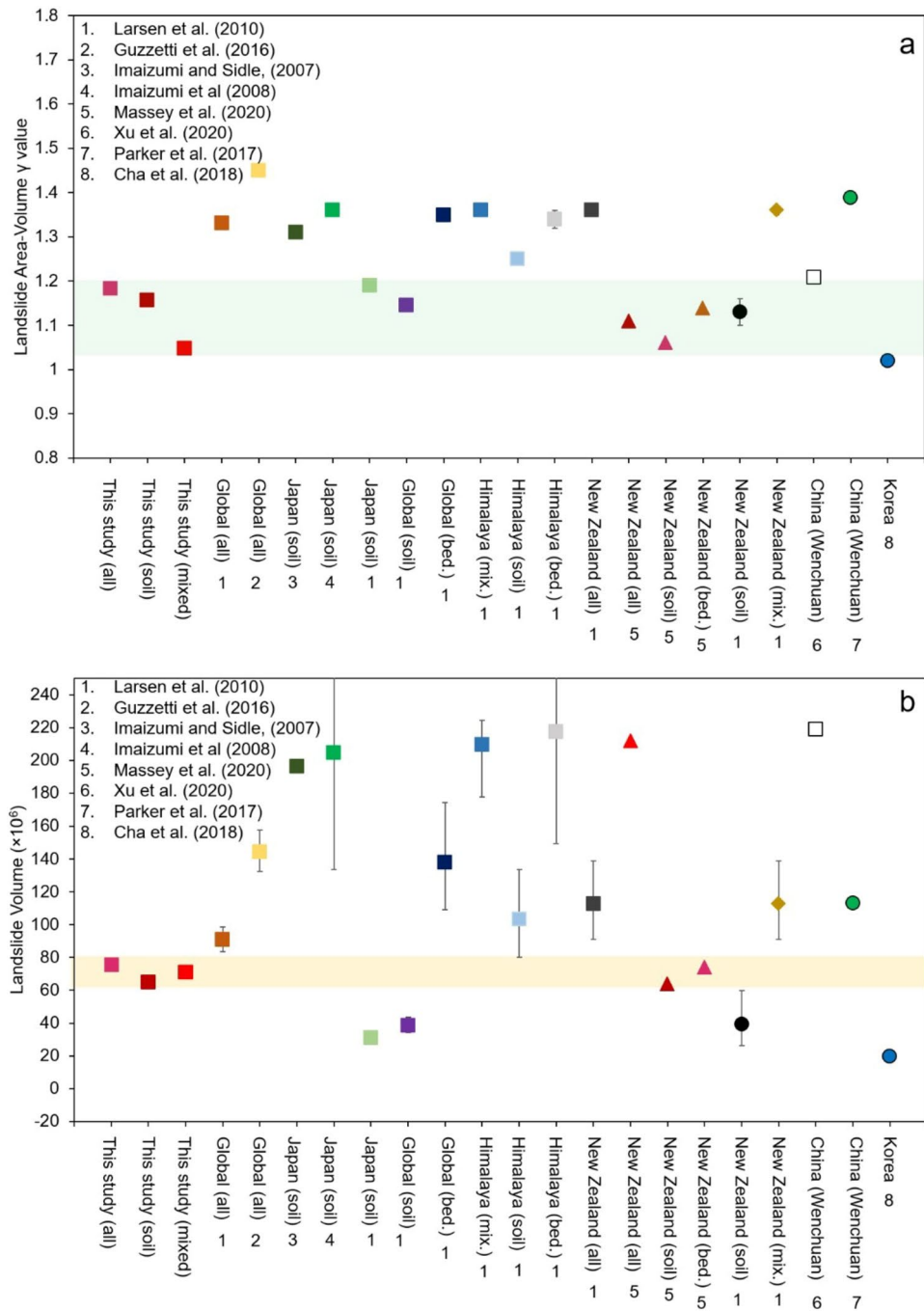


Figure 4. (a) Landslide area—volume scaling exponents (γ) obtained from this study and those studies listed in Table 1. (b) shows the total volume of debris produced by the Hokkaido Eastern Ibuli Earthquake estimated from the new area-volume relationship obtained in this study and those listed in Table.

was one of a kind in which the seismic pulse produced the largest number and volume of co-seismic landslides in mapping history. With this notion in mind, and to validate the Parker et al.³ findings, we compare the net uplift volume of the 2018 Hokkaido Eastern Ibuli Earthquake event, and the net erosion volume caused by landslides in our testing area. The calculated net uplift volume in the study area ($\sim 512 \text{ km}^2$: testing site) was found to be 5.55 million m^3 . On the other hand, widespread landsliding produced 64–72 million m^3 of debris from the affected catchments, which is found to be much greater than the estimated net uplift volume of 5.55 million m^3 . Our results seem to agree with the Parker et al.³ results and suggest that frequent large earthquakes may counterbalance the topographic uplift through erosion by landslides. This simple straightforward analysis may have overlooked isostatic compensation, inter-seismic vertical movement, and flexural rigidity of the lithosphere⁴⁶; hence should be interpreted with caution. Nonetheless, Hovius et al.⁴⁷ reported that $\sim 840 \text{ Mt}$ of sediment had been moved out of the Choshui catchment in Taiwan following the Chi-Chi earthquake of 1999 until up to 2007,

equaling to 4/5th of the rock mass added by the earthquake. Adding the background erosion rate in the region by rainfall and typhoons, their work also concluded that the tectonic mass flux added into the orogenic systems can be countered by landslides in a few years.

Conclusions

The 2018 Hokkaido Eastern Iburi earthquake caused a large number of landslides in more than 500 km² area. Using 1 m LiDAR elevation models, we calibrated an area-volume power-law for landslides and found that the values of γ exponent (1.15–1.18) for the 1719 predominantly soil landslides initiated by this earthquake lies within the centre of the range of γ values reported for soil landslides in the literature. However, we noticed large deviations in the total estimates of debris volume from existing area-volume relationships. We attribute this discrepancy to contrasting methods and mapping inaccuracies due to low-resolution DEMs used in previous studies. Failure to account for source and deposit areas, and the amalgamation of small landslide clusters can also significantly contribute to overestimating the total volume, leading to incorrect estimates. Results of the present study show that the net uplift produced by this earthquake deformation is smaller than the total eroded volume produced by co-seismic landslides.

Data availability

The airborne LiDAR-derived digital elevation models presented in the paper were originally provided by geospatial information of Hokkaido and the processed DEM files and mapped landslides are available from <https://doi.org/10.6084/m9.figshare.21858687> and <https://doi.org/10.6084/m9.figshare.21858726>, respectively.

Received: 16 February 2023; Accepted: 12 May 2023

Published online: 19 May 2023

References

1. Fan, X. *et al.* Earthquake-Induced chains of geologic hazards: Patterns, mechanisms, and impacts. *Rev. Geophys.* **57**, 421–503 (2019).
2. Li, G. *et al.* Seismic mountain building: Landslides associated with the 2008 Wenchuan earthquake in the context of a generalized model for earthquake volume balance. *Geochem. Geophys. Geosyst.* **15**, 833–844 (2014).
3. Parker, R. N. *et al.* Mass wasting triggered by the 2008 Wenchuan earthquake is greater than orogenic growth. *Nat. Geosci.* **4**(7), 449–452 (2011).
4. Malamud, B. D., Turcotte, D. L., Guzzetti, F. & Reichenbach, P. Landslides, earthquakes and erosion. *Earth Planet. Sci. Lett.* **229**, 45–59 (2004).
5. Koi, T. *et al.* Prolonged impact of earthquake-induced landslides on sediment yield in a mountain watershed: The Tanzawa region, Japan. *Geomorphology* **101**, 692–702 (2008).
6. Catani, F., Tofani, V. & Lagomarsino, D. Spatial patterns of landslide dimension: A tool for magnitude mapping. *Geomorphology* **273**, 361–373 (2016).
7. Tacconi Stefanelli, C., Casagli, N. & Catani, F. Landslide damming hazard susceptibility maps: a new GIS-based procedure for risk management. *Landslides* **17**, 1635–1648 (2020).
8. Liu, J. *et al.* Ecosystem carbon stock loss after a mega earthquake. *Catena (Amst)* **216**, 106393 (2022).
9. Hilton, R. G., Galy, A. & Hovius, N. Riverine particulate organic carbon from an active mountain belt: Importance of landslides. *Glob. Biogeochem. Cycles* **22**, (2008).
10. Yunus, A. P. *et al.* Decadal vegetation succession from MODIS reveals the spatio-temporal evolution of post-seismic landsliding after the 2008 Wenchuan earthquake. *Remote Sens Environ* **236**, 111476 (2020).
11. Gabet, E. J. A theoretical model coupling chemical weathering and physical erosion in landslide-dominated landscapes. *Earth Planet Sci. Lett.* **264**, 259–265 (2007).
12. Massey, C. I. *et al.* Volume characteristics of landslides triggered by the MW 7.8 2016 Kaikōura Earthquake, New Zealand, derived from digital surface difference modeling. *J. Geophys. Res. Earth Surf* **125**, e2019JF005163 (2020).
13. Samia, J. *et al.* Do landslides follow landslides? Insights in path dependency from a multi-temporal landslide inventory. *Landslides* **14**, 547–558 (2017).
14. Ozturk, U. *et al.* How robust are landslide susceptibility estimates?. *Landslides* **18**, 681–695 (2021).
15. Tang, C. *et al.* Analysing post-earthquake mass movement volume dynamics with multi-source DEMs. *Eng. Geol.* **248**, 89–101 (2019).
16. Dai, L. *et al.* Coseismic debris remains in the orogen despite a decade of enhanced landsliding. *Geophys. Res. Lett.* **48**, e2021GL095850 (2021).
17. Simonett, D. S. Landslide distribution and earthquakes in the Bewani and Torricelli Mountains, New Guinea In *Landform studies from Australia and New Guinea* (eds Jennings, J. A. *et al.*) 64–84 (Cambridge University Press, 1967).
18. Chen, S., Chen, C. & Huang, W. Exploring landslide erosion volume–area scaling relationships by slip depth using changes in DTMs for basin sediment volume estimation. *J. Mt. Sci.* **16**, 581–594 (2019).
19. Brunetti, M. T., Guzzetti, F. & Rossi, M. Probability distributions of landslide volumes. *Nonlinear Process Geophys.* **16**, 179–188 (2009).
20. Xu, C. *et al.* Optimized volume models of earthquake-triggered landslides. *Sci. Rep.* **1**(6), 1–9 (2016).
21. Imaizumi, F. & Sidle, R. C. Linkage of sediment supply and transport processes in Miyagawa Dam catchment, Japan. *J. Geophys. Res. Earth Surf.* **112**, 1–17 (2007).
22. Larsen, I. J., Montgomery, D. R. & Korup, O. Landslide erosion caused by hillslope material. *Nature Geosci.* **3**, 247–251 (2010).
23. Zhuang, J. *et al.* Empirical relationships of the landslides in the Chinese Loess Plateau and affect factors analysis. <http://www.tandfonline.com/action/journalInformation?show=aimsScope&journalCode=tgnh20#VsXodSCLRhE> **13**, 250–266 (2022).
24. Hovius, N. & Stark, C. P. Landslide-driven erosion and topographic evolution of active mountain belts. *Landslides from Massive Rock Slope Failure* 573–590 (2006). https://doi.org/10.1007/978-1-4020-4037-5_30.
25. Li, G., West, A. J. & Qiu, H. Competing effects of mountain uplift and landslide erosion over earthquake cycles. *J. Geophys. Res. Solid Earth* **124**, 5101–5133 (2019).
26. Valagussa, A., Frattini, P., Valbuzzi, E. & Crosta, G. B. Role of landslides on the volume balance of the Nepal 2015 earthquake sequence. *Sci. Rep.* **11**, 1–12 (2021).
27. Dou, J. *et al.* Different sampling strategies for predicting landslide susceptibilities are deemed less consequential with deep learning. *Sci. Total Environ.* **720**, 137320 (2020).

28. Wang, F., Fan, X., Ph, D., Felipe, A. & Rodriguez, A. Landslides Coseismic landslides triggered by the 2018 Hokkaido, Japan (Mw 6.6) earthquake: Spatial distribution, controlling factors and possible failure mechanism (2018).
29. GSI. *Slope failure/sedimentation distribution map GeoJSON (Geospatial Information Authority of Japan technical data D1-No.991)*. <https://www.gsi.go.jp/BOUSAI/H30-hokkaidoiburi-east-earthquake-index.html#10> (2018).
30. Nava, L., Bhuyan, K., Meena, S. R., Monserrat, O. & Catani, F. Rapid mapping of landslides on SAR data by attention U-net. *Remote Sens.* **14**, 1449 (2022).
31. Frodella, W., Yang, Z. & Xu, C. Efficient Detection of Earthquake-Triggered Landslides Based on U-Net: An Example of the 2018 Hokkaido Eastern Iburu (Japan) Mw = 6.6 Earthquake. *Remote Sensing* **2022**, Vol. 14, 2826 (2022).
32. Ishikawa, T., Yoshimi, M., Isobe, K. & Yokohama, S. Reconnaissance report on geotechnical damage caused by 2018 Hokkaido Eastern Iburu earthquake with JMA seismic intensity 7. *Soils Found.* **61**, 1151–1171 (2021).
33. Kawamura, S., Kawajiri, S., Hirose, W. & Watanabe, T. Slope failures/landslides over a wide area in the 2018 Hokkaido Eastern Iburu earthquake. *Soils Found.* **59**, 2376–2395 (2019).
34. Nakagawa, M., Amma-Miyasaka, M., Miura, D. & Uesawa, S. Tephrostratigraphy in Ishikari Lowland, Southwestern Hokkaido. *J. Geol. Soc. Jpn* **124**, 473–489 (2018).
35. Pelletier, J., Broxton, P., Hazenberg, P., DAAC, X. Z.-O. & 2016, undefined. Global 1-km gridded thickness of soil, regolith, and sedimentary deposit layers. daac.ornl.gov.
36. Guzzetti, F., Ardizzone, F., Cardinali, M., Rossi, M. & Valigi, D. Landslide volumes and landslide mobilization rates in Umbria, central Italy. *Earth Planet. Sci. Lett.* **279**, 222–229 (2009).
37. Imaizumi, F., Sidle, R. C. & Kamei, R. Effects of forest harvesting on the occurrence of landslides and debris flows in steep terrain of central Japan. *Earth Surf. Process Landf.* **33**, 827–840 (2008).
38. Cha, D., Hwang, J. & Choi, B. Landslides detection and volume estimation in Jinbu area of Korea. <https://doi.org/10.1080/21580103.2018.144636714,61-65> (2018).
39. Osanai, N. *et al.* Characteristics of landslides caused by the 2018 Hokkaido Eastern Iburu Earthquake. *Landslides* **16**, 1517–1528 (2019).
40. Yamagishi, H. & Yamazaki, F. Landslides by the 2018 Hokkaido Iburu-Tobu Earthquake on September 6. *Landslides* **15**, 2521–2524 (2018).
41. MLIT. *Response to disasters on the 2018 Hokkaido Eastern Iburu Earthquake* (in Japanese). http://www.mlit.go.jp/river/sabo/h30_iburitobu/181005_sediment_volume.pdf (2018).
42. Yang, F. *et al.* Catastrophic debris flows triggered by the 20 August 2019 rainfall, a decade since the Wenchuan earthquake, China. *Landslides* **18**, 3197–3212 (2021).
43. Bhuyan, K. *et al.* Mapping landslides through a temporal lens: an insight toward multi-temporal landslide mapping using the u-net deep learning model. <https://doi.org/10.1080/15481603.2023.218205760,1> (2023).
44. Scheip, C. M. & Wegmann, K. W. HazMapper: A global open-source natural hazard mapping application in Google Earth Engine. *Nat. Hazard.* **21**, 1495–1511 (2021).
45. Avouac, J. Crustal and Lithosphere Dynamics. Preprint at (2008).
46. Molnar, P. Isostasy can't be ignored. *Nat. Geosci.* **5**(2), 83–83 (2012).
47. Hovius, N. *et al.* Prolonged seismically induced erosion and the mass balance of a large earthquake. *Earth Planet. Sci. Lett.* **304**, 347–355 (2011).

Acknowledgements

The authors would like to thank the Gspatial Information of Hokkaido for providing the open topographic data. We further thank Hokkaido Forest Research Institute for help in the field survey. This work was partially supported by Kajima Foundation Grant and Grant-in-Aid for Scientific Research (C) 21K05664. Mr. Chen Xinyu would like to thank DX Scholarship (JST SPRING—No: JPMJSP2119), Hokkaido University. The authors are grateful for the guidance and data access support provided by Dr. Yuichi Hayakawa. Authors also thank the editor and reviewers for their constructive suggestions.

Author contributions

Y.A.P, R.A and C.X designed the study and conducted formal analysis. A.G, X.C, R.A and Y.A.P conducted the field work. Y.A.P, and S.S prepared the figures with help from C.S and R.A. F.C, X.F and S.K contributed in the interpretation of data. R.A and C.X obtained the funding. All authors discussed the results and contributed to the writing and review of the final manuscript.

Competing interests

The authors declare no competing interests.

Additional information

Correspondence and requests for materials should be addressed to R.A.

Reprints and permissions information is available at www.nature.com/reprints.

Publisher's note Springer Nature remains neutral with regard to jurisdictional claims in published maps and institutional affiliations.



Open Access This article is licensed under a Creative Commons Attribution 4.0 International License, which permits use, sharing, adaptation, distribution and reproduction in any medium or format, as long as you give appropriate credit to the original author(s) and the source, provide a link to the Creative Commons licence, and indicate if changes were made. The images or other third party material in this article are included in the article's Creative Commons licence, unless indicated otherwise in a credit line to the material. If material is not included in the article's Creative Commons licence and your intended use is not permitted by statutory regulation or exceeds the permitted use, you will need to obtain permission directly from the copyright holder. To view a copy of this licence, visit <http://creativecommons.org/licenses/by/4.0/>.

© The Author(s) 2023